RSC Advances

PAPER

View Article Online
View Journal | View Issue

Cite this: *RSC Adv.*, 2023, **13**, 13516

Developing novel imidazoline-modified glucose derivatives as eco-friendly corrosion inhibitors for Q235 steel

Weijun Qi,[a] Yu Huang,[a] Yuting Ma,[a] Zizhou Yu[ac] and Xinbao Zhu *[ab]

Many natural compounds and imidazoline derivatives have been previously evaluated as eco-friendly corrosion inhibitors for application in the food, pharmaceutical and chemical industries. Herein, a novel alkyl glycoside cationic imaginary ammonium salt (FATG) was designed *via* the grafting of imidazoline molecules into the skeleton of a glucose derivative, and its effects on the electrochemical corrosion behavior of Q235 steel in 1 M HCl were systemically investigated by electrochemical impedance spectroscopy (EIS), potentiodynamic polarization curves (PDP), and gravimetric measurements. The results indicated that its maximum inhibition efficiency (IE) was 96.81% at a concentration as low as 500 ppm. The adsorption of FATG on the Q235 steel surface followed the Langmuir adsorption isotherm. The scanning electron microscopy (SEM) and diffraction X-ray (XRD) results suggested the formation of inhibitor film on the metal surface, which significantly impeded the corrosion of Q235 steel. Additionally, FATG showed a high biodegradability efficiency (98.4%), which had great potential as a green corrosion inhibitor based on concepts of greenness and biocompatibility.

Received 11th January 2023
Accepted 27th March 2023

DOI: 10.1039/d3ra00222e

rsc.li/rsc-advances

1 Introduction

Acid-driven corrosion is mainly caused by acidic materials that react with metallic surfaces, primarily causing the corrosion of steel structures such as buildings, high-value assets, working machines and statues, which also indirectly affect industrial sectors and even human health.[1] Various approaches, including adding corrosion inhibitors,[2] surface modification, anticorrosive coatings[3] and electrochemical means[4] have been carried out to address this issue. Among them, due to their excellent adsorbability and structure stability, the use of corrosion inhibitors, such as imidazoline derivatives,[5–7] thiourea derivatives,[8] isoxazolium derivatives,[9] inorganic chromates,[10] and organophosphorus derivatives,[11] has been considered as an economical, efficient and versatile strategy to improve the corrosion-resistance of metals. Despite their popularity, most of these derivatives also negatively impact the environmental profile. In contrast, natural resources, such as those extracted or modified from plants or agro-industrial waste, for instance, coffee bagasse oil,[12] rice bran oil,[13,14] wasted mango seeds,[15] wasted avocado oil,[16] and Rosa canina fruit,[17] have been used to synthesize corrosion inhibitors and have received great attention due to their non-toxicity, biodegradability, and they have no negative influence on the environment.[18] However, problematic extraction and storage still limit their large-scale commercialization.

Carbohydrates, such as chitosan,[19] starch,[20] exudate gums,[21] and glucose,[22–24] have great potential as feedstocks for corrosion inhibitor material because of their high molecular weight, and high adsorption performance.[25–27] Among them, glucose exhibits more excellent solubility performance as compared to others since it bears numerous polar functional groups. Additionally, it is more cost-effective and easily obtainable from natural sources. Unfortunately, glucose by itself could fail to achieve a good inhibiting effect, therefore, Wang *et al.*[22] have reported that thiocarbohydrazide was introduced to glucose to increase its corrosion inhibition performance. Additionally, the presence of alkyl glycosides might increase the adsorption sites due to numerous hydroxyl groups promoting adsorption and increasing the coverage on the steel surface to improve the inhibition performance.

Monomer acid (MA), shows great potential for the development of high-value products such as imidazoline due to its eco-friendly, cost-effective, abundant and easily accessible[28] properties. In general, it is a good source of high-quality fatty acids since it contains stearic acid, octadecenoic acid, palmitic acid and oleic acid. Unfortunately, MA, an inexpensive by-product of the manufacturing of dimer acid, has not attracted enough attention, even though it has been commonly used in some fields.[29,30] As far as we know, no research has focused on the preparation of an acceptable corrosion inhibitor from waste MA.

[a]*Jiangsu Co-Innovation Center of Efficient Processing and Utilization of Forest Resources, College of Chemical Engineering, Nanjing Forestry University, Nanjing 210037, China. E-mail: zhuxinbao@njfu.com.cn*

[b]*Jiangsu Province Key Laboratory of Green Biomass-based Fuels and Chemicals, Nanjing 210037, China*

[c]*Yangzhou Chenhua New Material Co., Ltd, Yangzhou, 225800, China*

In this context, synthesized glucose derivatives of novel acceptable corrosion inhibitors featured in inexpensive raw materials and green production are an excellent solution to the problem of corrosion. Herein, we report the synthesis of a novel alkyl glycoside cationic imaginary ammonium salt, (FATG) from modified glucose and waste MA. The target of this research was to develop a novel surfactant that could be used as a green inhibitor for the HCl corrosion of Q235 steel. Potentiodynamic polarization (PDP) and electrochemical impedance spectroscopy (EIS) techniques have been applied to the study of inhibitory behavior. The adsorption behavior of the inhibitor on the Q235 steel surface has been studied through density functional theory (DFT) to explain the mechanism of adsorption, further offering theoretical information for designing and synthesizing novel inhibitors.

2 Experiments and methods

2.1 Material

N-(2-Aminoethyl) ethanolamine (AR), chlorinated alkyl glycosides,[31] monomeric acid (wt%: palmitic acid 23.10, oleic acid 31.24, stearic acid 37.13, octadecadienoic acid 4.73, and arachidic acid 3.62) were used to synthesize the imidazoline derivative inhibitors. All of these materials were directly used without further purification.

The chemical composition of Q235 steel is given in Table 1. The steel was mechanically cut into 10 mm × 10 mm × 0.5 mm coupons. Prior to the corrosion test, the working surface was scraped with 1200-grade abrasive paper, washed, and degreased with deionized water.

2.2 Synthesis and evaluation of imidazoline inhibitors

As shown in Fig. 1, the FATG was prepared *via* a series of reactions. Here, 0.5 mol MA and 0.8 mol *N*-(2-hydroxyethyl)ethylenediamine were added to the reactor, heated from 150 °C to 230 °C until no more water came from the water segregator, and then steamed. Subsequently, 0.5 mol chloroalkyl glycoside and 10 mL methanol were added to the reactor. The reaction was kept at 80 °C for 5 h to obtain a light brown crude product, which was then extracted in EtOAc-*n*-hexane for further purification.

The FATG was characterized by FTIR (German VERTEX 80V) between 4000 and 500 cm^{-1}, ^1H NMR, and ^{13}C NMR.

2.3 Inhibition performance of synthesized inhibitors

Gravimetric experiments were conducted to determine the corrosion rate of the metal hanging sheet before and after studying the corrosion mass change to judge the corrosion resistance of the material. The previously weighed Q235 steel strips of size 10 mm × 10 mm × 0.5 mm with a total exposed area of 2 cm^2 were dried and then immersed in 100 mL of 1 M HCl without and with different concentrations of FATG inhibitors for 6 h. Also, considering the effect of the corrosive medium temperature on the inhibition efficiency of FATG, gravimetric experiments were carried out at temperatures ranging from 298 K to 338 K.

The inhibition performance of the synthesized inhibitors in 1 M HCl solution was investigated by electrochemical measurements, which were carried out in a Corrtest CS2350H electrochemical workstation with a three-electrode system including the working electrode (Q235 steel), auxiliary electrode (platinum electrode), and a reference electrode (saturated calomel electrode). The working electrode was shielded with silica gel and an uncovered zone of 1 cm^2 was the test surface. Before the test, the working surface was immersed in 1 M HCl solution for 1 h.

Electrochemical impedance spectroscopy (EIS) tests were conducted with a 10 mV AC disturbance to obtain the amplitude, setting the frequency range from 100 kHz to 0.05 Hz. Potentiodynamic polarization curves (PDP) were obtained after EIS tests with a 2 mV s^{-1} scanning rate from −1.0 to 0.2 V *vs.* SCE.[32] As mentioned above, the operations should not be started until the open circuit is stable.

Table 1 Chemical composition of Q-235 steel

Fe	C	Si	Mn	P	S	Cr	Ni	Al
Bal.	0.012	0.001	0.001	0.011	0.008	0.01	0.001	0.006

2.4 Characterizations of surface films

The inhibited surface morphology and element distribution of Q235 steel immersed without or with 500 ppm FATG for 7 days

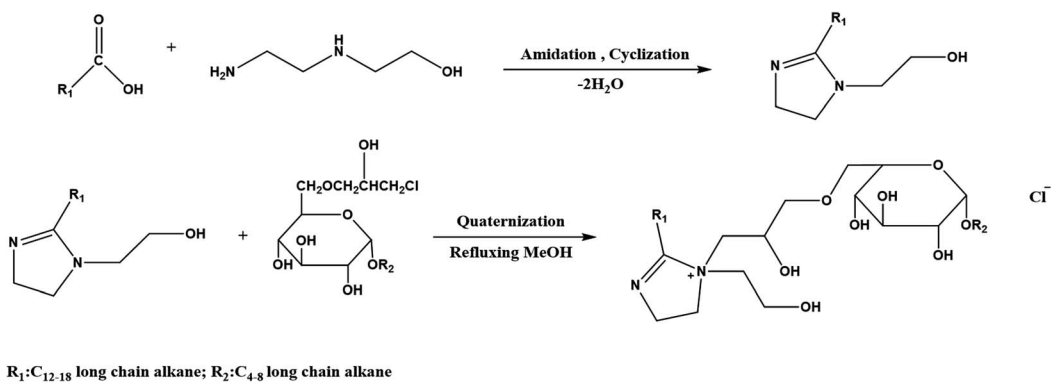

Fig. 1 Synthesis route of FATG.

were determined with an FEI Quanta 200 scanning electron microscope (SEM-EDX). Prior to SEM observation, the specimens were taken from the 1 M HCl solution and gently scrubbed, washed with deionized water, and dried under gas streams. X-ray diffraction (XRD) was used as an effective method to analyse the crystal structures of corrosion products. Steel sheets were tested under the conditions of a scattering angle range of $2\theta = 10$ to 80°.

2.5 Biodegradability study

The degradation behavior of FATG was investigated by the test method for the biodegradability of surfactants (GB/T 15818-2018). The cultured activated sludge of the surfactant samples was used as the biodegradation source, which was added to the test part of the oscillating culture. The reduction of the surfactant during the culture period was measured, and the biodegradability of the specified time was obtained.

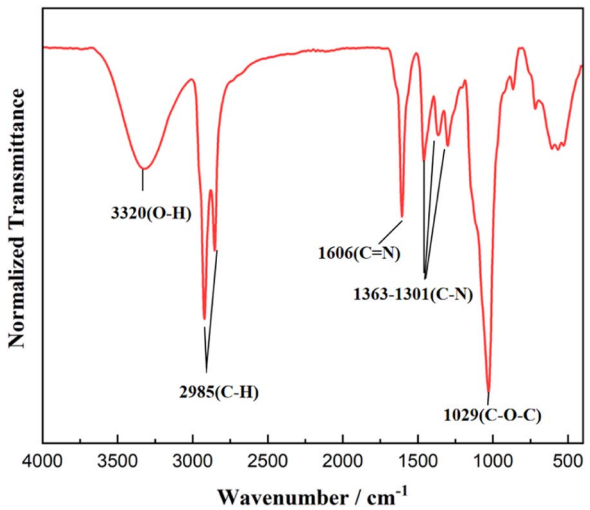

Fig. 2 Infrared spectra of FATG.

2.6 Quantum chemistry calculation

The quantum chemical calculations were conducted using the DFT-based program Gaussian 09W at the B3LYP/6-31G(d,p) basis set. The solvent (water) effect was considered. Geometry optimization was performed, and the highest occupied molecular orbital (E_{HOMO}), lowest unoccupied molecular orbital (E_{LUMO}), and other parameters were determined.[33–35]

3 Results and discussion

3.1 Characterization of FATG

The FTIR spectrum of FATG is shown in Fig. 2. The absorption peak at about 3320 cm^{-1} corresponds to the stretching vibration peak of O–H. The characteristic peak at about 1606 cm^{-1} was observed in the spectra of products, which matched the C=N double bond stretching vibration.[15,36] The absorption peaks at about 1363 cm^{-1} and 1301 cm^{-1} were due to the C–N vibrations.[22,37] A new strong band at 1029 cm^{-1} was attributed to the C–O–C vibration, suggesting that an alkyl glycoside structure was present in the imidazoline structure. The FT-IR results also revealed that imidazoline was successfully synthesized. ^{1}H NMR and ^{13}C NMR spectra are displayed in Fig. 3 to further confirm the structure. For FATG, ^{1}H NMR (600 MHz, chloroform-d) δ 5.39 (s, 1H, C–OH), 4.84 (s, 1H, C–OH), 4.24 (s, 2H, CH_2–O), 3.91 (s, 4H, N–CH_2), 3.80 (s, 2H, N–CH_2), 3.78-3.48 (m, 8H, GluCH/CH=N/CH_2–O), 3.45 (d, J = 26.7 Hz, 4H, CH_2–O), 2.58 (s, 2H, C=N–CH_2), 1.97 (s, 2H, CH_2), 1.60 (s, 4H, CH_2), 1.26 (s, 30H, CH_2), 0.89 (s, 6H, CH_3). ^{13}C NMR (151 MHz, $CDCl_3$) δ 151.30, 142.70, 110.25, 109.33, 78.43, 77.11, 71.21, 69.91, 65.17, 50.76, 44.13.[6,37–39]

3.2 Gravimetric measurements

The weight loss-time data, as depicted in Table 2, revealed that the FATG inhibitor acted as a good inhibitor when Q235 steel was immersed in 1 M HCl solution for 6 h at temperatures

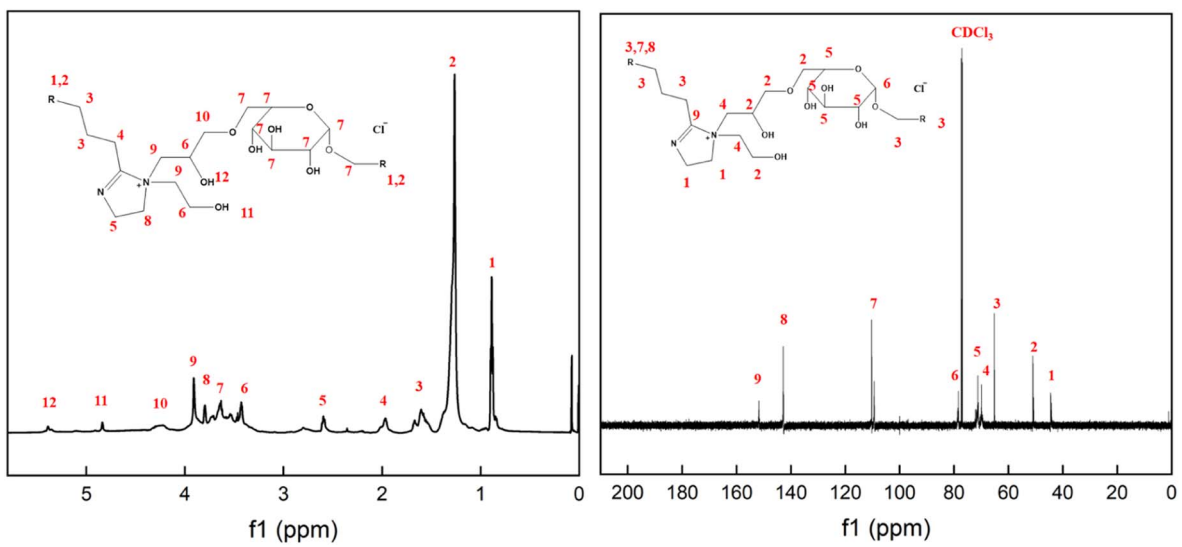

Fig. 3 ^{1}H NMR spectra and ^{13}C NMR spectra of FATG.

Table 2 Corrosion parameters for Q235 steel in 1 M HCl in the absence and presence of different concentrations of FATG at 298–338 K from weight loss measurements

Inhibitor com. (ppm)	Weight loss (mg cm^{-2})					Corrosion inhibition efficiency of FATG (%)				
	298 K	308 K	318 K	328 K	338 K	298 K	308 K	318 K	328 K	338 K
Blank	7.3	16.4	29.3	66.7	141.5	—	—	—	—	—
100	0.9	2.3	2.2	3.0	3.4	87.67	85.98	92.49	95.50	97.60
200	0.7	1.9	2.0	2.6	3.1	90.41	88.41	93.17	96.10	97.81
300	0.6	1.4	1.9	2.2	2.5	91.78	91.46	93.52	96.70	98.23
400	0.5	1.3	1.6	1.1	2.8	93.15	92.07	94.54	98.35	98.02
500	0.3	1.0	1.4	1.0	2.1	95.89	93.90	95.22	98.50	98.52

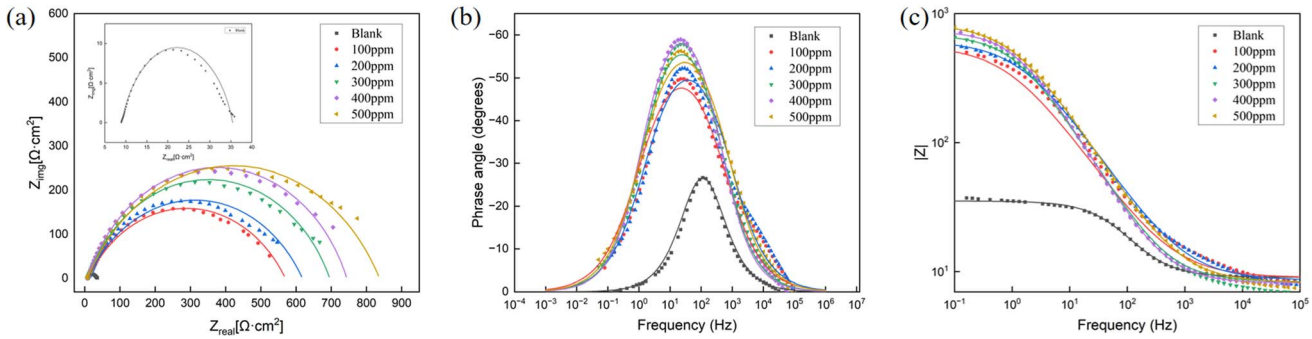

Fig. 4 Nyquist and Bode plots for Q235 steel in 1 M HCl solution without and with various concentrations of FATG at 298 K.

below 338 K. The inhibition efficiency in the presence of FATG increased with the increasing concentration of the inhibitor in 1 M HCl. The surface coverage was calculated using the following formula:[40]

$$\mathrm{EI}\% = \frac{W_0 - W_i}{W_0} \times 100\% \quad (1)$$

where W_0 is the weight loss in uninhibited acid solution and W_i is the weight loss in inhibited acid solution.

FATG demonstrated outstanding inhibiting properties at temperatures in the range of 298–338 K. It was apparent from the results that the corrosion inhibition efficiency of the inhibitor also depended on the factor of temperature. At room temperature, the FATG inhibitor formed a protective film through physical or chemical adsorption on the metal surface. Coincidentally, it was seen that the corrosion inhibition efficiency of the solution temperature gradually increased and was finally stabilized at around 98%, with the increase in solution temperature. It was seen that heating without an inhibitor would make the Fe atoms more likely to lose electrons and enter the solution in the form of Fe^{2+} to accelerate the dissolution of Q235 steel. Whereas, it was effective to add the inhibitor to slow the loss of metal weight. Based on the data, the phenomenon implied that chemisorption was the main mechanism when heated. Heating would accelerate the thermal movement of the inhibitor molecules on the metal surface to promote the formation of chemical bonding between them. This led to the inhibitor being firmly attached to the metal surface and it was difficult to desorb once it had been absorbed.[40–42]

3.3 EIS measurements

EIS measurements for Q235 steel dipped in a corrosive medium (1 M HCl solution) were plotted using Nyquist and Bode graphs in the absence and presence of various concentrations of FATG, as portrayed in Fig. 4. The Nyquist plot showed that the semicircular curves of the FATG increased with concentration in Fig. 4a. When an inhibitor concentration of 500 ppm was reached, the impedance value was the maximum. Moreover, in the EIS test of solid electrodes, the curve deviated from the semicircle trajectory to show a deformed semicircular shape, a phenomenon known as the "dispersion effect", which was generally considered to be caused by the active site of the metal surface being heterogeneous, or the poor conductivity of the solution.[43] Therefore, by combining the Nyquist and Bode diagrams obtained by the experiment, the equivalent circuit shown in Fig. 5 was selected to fit the impedance spectrum, and the fitted parameters are listed in Table 3.

The equivalent circuit model was simulated in Fig. 5, based on the EIS spectra of the FATG to further imitate the combined physical processes occurring at the metal electrode/electrolyte

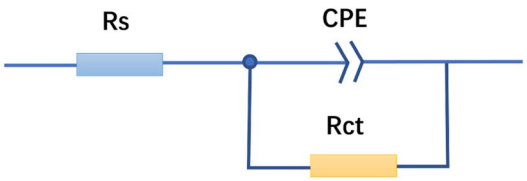

Fig. 5 Equivalent circuit for Q235 steel in 1 M HCl solution.

Table 3 Electrochemical parameters to fit the EIS data of Q-235 steel corroded in 1 M HCl solution containing different concentrations of FATG

		CPE			
Dose (ppm)	R_s (Ω cm^2)	Y_0 (S^n cm^{-2} Ω $\times$ 10^4)	n	R_{ct} (Ω cm^2)	EI/%
0	9.034	4.1127	0.72379	26.4	—
100	8.954	5.3684	0.65745	560.7	95.29
200	8.535	3.527	0.67273	609.5	95.67
300	8.313	3.2794	0.73724	687.3	96.16
400	8.144	2.8902	0.84314	736.1	96.41
500	8.185	3.092	0.80332	828.6	96.81

interface. The capacitive loop of the first quadrant was generated in parallel by resistance and capacitance.[43] From the Nyquist diagram, the starting point of the capacitive loop did not pass through the origin, indicating that there was a solution resistance in the electrolytic cell.[7] Moreover, in the equivalent circuit, CPE, an electrochemical element, was introduced to reflect the "dispersion effect", which could be used as a gauge of the heterogeneity or roughness of the FATG surface.[43–45] Therefore, the equivalent circuit shown in Fig. 5 was selected as the equivalent circuit. R_s is the solution resistance, R_{ct} is the charge transfer resistance, and CPE is the constant phase angle element.

Table 3 lists the electrochemical corrosion parameters of CPE (Y_0), the dispersion index (n), as well as the percentage inhibition efficiency (IE%), *etc.* The inhibition efficiency (IE%) was calculated from the following equation:[46]

$$\mathrm{IE}\% = \frac{R_{ct} - R_{ct,0}}{R_{ct}} \times 100\% \quad (2)$$

$R_{ct,0}$ and R_{ct} are the charge transfer resistance values without and with inhibitor, respectively. The fitting results are recorded in Table 3. The best inhibition efficiency was about 96.81% at the concentration of 500 ppm. With increasing concentration of the inhibitor, the R_{ct} value increased from 26.4 Ω cm^2 to 828.6 Ω cm^2. This could be because the imidazoline molecule could offer "attachment points" and adsorb on the metal surface, then, where they formed monomolecular layers, increase the shielding effect to promote the improvement of corrosion inhibition efficiency. Moreover, the increase in the n-value after adding the FATG inhibitor in the corrosive solution could facilitate the reduction of surface inhomogeneity due to the adsorption of inhibitor molecules on the most active adsorption sites at the surface.[47] Generally, when there was a diffusion effect on the electrode surface, the value of n was always between 0.5 and 1, which was consistent with the fitting results.

3.4 PDP measurements

The Tafel curves recorded for Q235 steel in 1 M HCl solution at various concentrations in the presence and absence of FATG inhibitor are shown in Fig. 6. The change in the self-corrosion potential was insignificant so it was considered that the cationic imidazoline belonged to a mixed-type corrosion inhibitor, with anodic oxidative dissolution corrosion and cathodic depolarization reduction being similarly impeded in

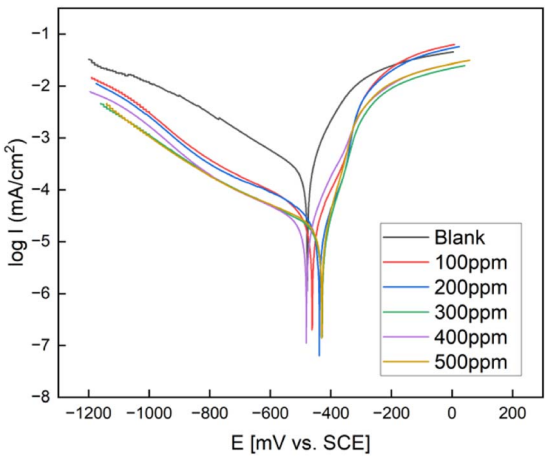

Fig. 6 Polarization curves of Q235 steel in 1 M HCl solution without and with various concentrations of inhibitor.

the electrolytic cell.[44,46,48] In addition, it was apparent that the corrosion rate of the Q235 steel was slowed down due to the corrosion current density (I_{corr}) dropping significantly to a lower value. The current density of the anodic polarization curve increased sharply in the later stages, developing a "plateau" as the corrosion inhibitor underwent desorption behavior on the metal surface. It can be seen that the synthesized FATG is an adsorption-type corrosion inhibitor, and a dynamic equilibrium was formed between adsorption and desorption.[46]

Table 4 lists the corrosion potential (E_{corr}), anode and cathode Tafel ramps (β_a and β_b), corrosion current density (I_{corr}), surface coverage (θ), as well as percentage rejection rate (IE%) electrochemical corrosion parameters. The inhibition efficiency was calculated based on the following equation:

$$\mathrm{IE}\% = \frac{I_{corr,0} - I_{corr}}{I_{corr,0}} \times 100\% \quad (3)$$

where $I_{corr,0}$ and I_{corr} are corrosion current densities in solution without and with inhibitor, respectively.

As shown in Table 4, as the concentration increased, the corrosion current density (I_{coor}) remarkably dropped to a lower value, and the best inhibition efficiency (IE%) was about 96.67% at a concentration of 500 ppm, showing excellent corrosion inhibition performance. At the same time, the corrosion potential (E_{corr}) and the Tafel slope (β_a and β_b) changed slightly,

Table 4 Electrochemical parameters and inhibition efficiency obtained from polarization curves for Q-235 steel immersed in 1 M HCl solution containing FATG

Dose/ppm	E_{coor}/mV	β_a/(mV dec^{-1})	β_b/(mV dec^{-1})	I_{coor}/(μA cm^{-2})	IE/%
0	−473.83	118.24	286.19	562.58	—
100	−461.52	74.878	365.09	27.654	95.08
200	−480.75	88.574	380.12	25.182	95.52
300	−437.82	64.945	206.72	23.715	95.78
400	−429.01	71.629	204.16	19.556	96.52
500	−429.68	71.099	232.16	18.747	96.67

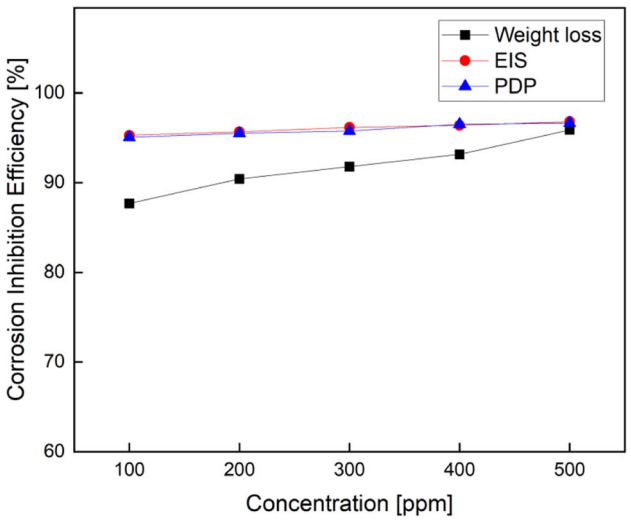

Fig. 7 Variation of the inhibition efficiency from three different techniques.

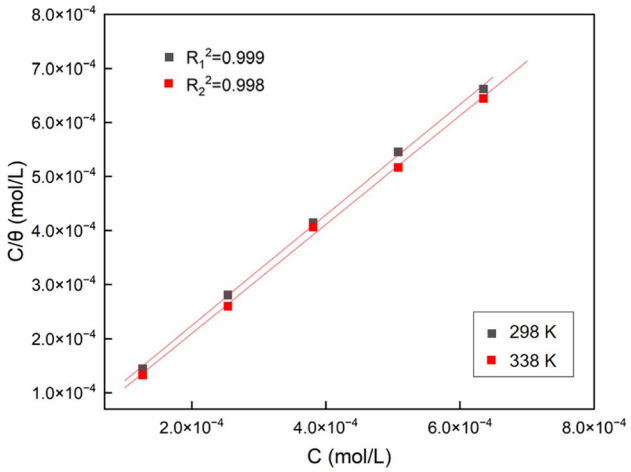

Fig. 8 Langmuir adsorption isotherm for Q235 steel in 1 M HCl solution.

suggesting that the synthesized FATG did not affect the reactions of both the anode and cathode, whose corrosion inhibition mechanism was to form a protective film on the surface of steel carbon and inhibit the active site of the reaction.[34]

The variation of the inhibition efficiency with the (FATG) inhibitor concentration at room temperature was calculated using three different techniques and is presented in Fig. 7.

3.5 Adsorption isotherm and thermodynamic parameters

The way adsorption occurs on metal surfaces could be clarified by making use of adsorption isotherms. Among the different models,[34] the best fit was obtained with the Langmuir model, shown in Fig. 8, according to the following equation:[48]

$$\frac{\theta}{1-\theta} = K_{ads}C \quad (4)$$

where K_{ads} is the adsorption equilibrium constant. This constant has some connection with the standard free energy of adsorption (ΔG_{ads}) according to the following equation:[49]

$$\Delta G^0_{ads} = -RT\ln(55.5K_{ads}) \quad (5)$$

where R is the universal gas constant and T is the absolute temperature. The value of 55.5 is the concentration of water in the solution in molarity units.

As shown in Fig. 8, the adsorption of FATG in solution at 298 K and 338 K accorded with the Langmuir adsorption isotherm with correlation factors $R_1^2 = 0.999$ and $R_2^2 = 0.998$. It can be concluded that the adsorption mode of corrosion inhibitor molecules on the electrode surface was likely to be monolayer adsorption, and the interaction force between adsorbed molecules could be ignored. Moreover, the values of ΔG_{ads} ($\Delta G_{ads1} = -38.11$ kJ mol^{-1} and $\Delta G_{ads2} = -39.76$ kJ mol^{-1}) implied that the adsorption process of the FATG on the Q235 steel surface was spontaneous and worked with physisorption and chemisorption.[50,51]

3.6 Surface analysis

Fig. 9a and b show that without the inhibitor, the Q235 steel surface was heavily concave and pitted. In the presence of the FATG compound, shown in Fig. 9c and d, the surface of Q235 steel images retained intact scratches, maximizing the protection of the iron surface against acid corrosion. Thus, we concluded that the inhibitor could be stably present in the system and build a defensive shield on the steel surface.[7,42] Furthermore, it was shown that Q235 was oxidized in an acidic solution, producing C and O from the EDX microchemical analysis. Comparing the two sets of reactions in Fig. 9e and f, in the presence of 500 ppm of inhibitor, the amount of C and O on the corroded steel was lower. Correspondingly, the content of Fe remained higher (96.6%), indicating that the inhibitor could effectively prevent the oxidation of Q235 steel.[22,52,53]

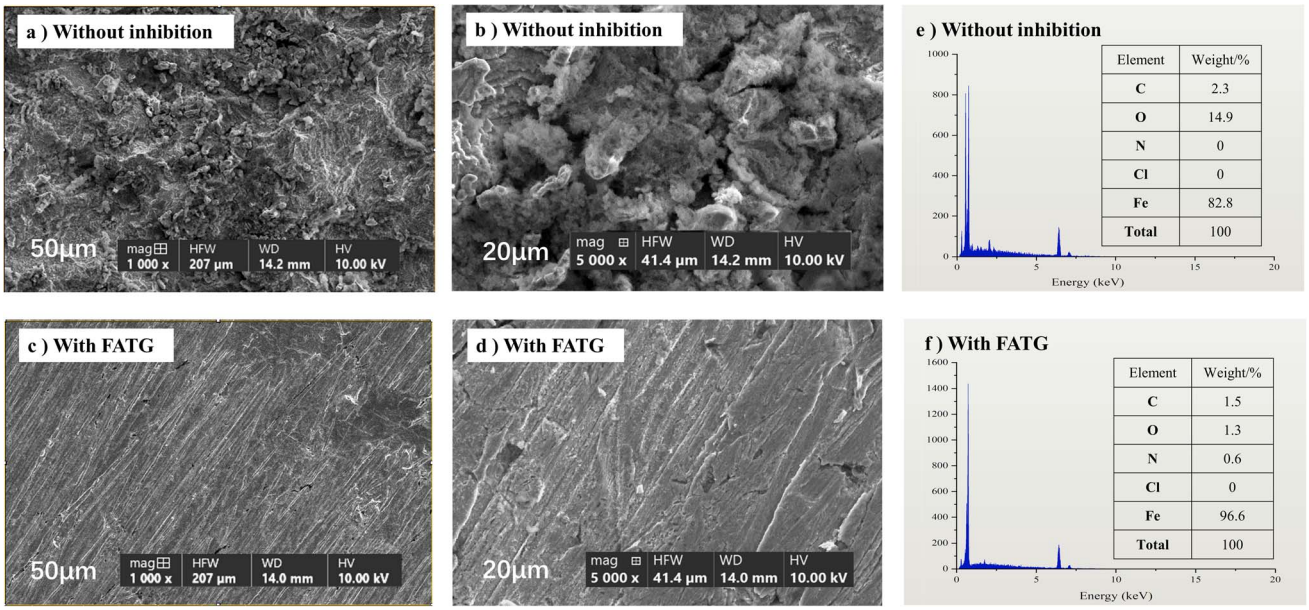

Fig. 9 SEM (a–d) and EDX (e and f) images of the sample after corrosion without or with 500 ppm FATG for 7 days.

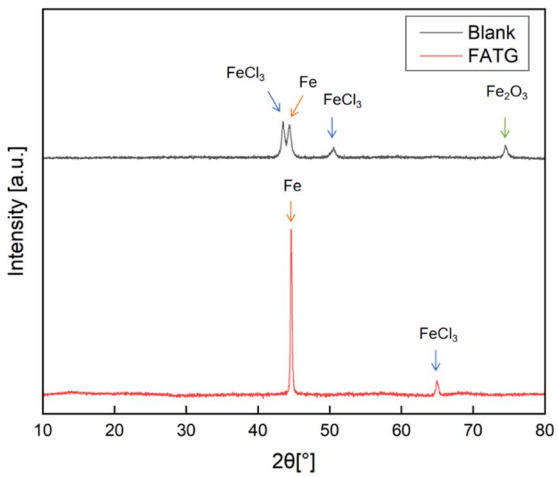

Fig. 10 XRD image of the sample after corrosion in the medium without or with 500 ppm of FATG for 48 h at 298 K.

The XRD pattern in Fig. 10 shows that at room temperature, the crystal structures of corrosion products formed on the surface of Q235 steel were mainly $FeCl_3$ and Fe_2O_3. Without the protection of the inhibitor, Q235 steel in an acidic solution was naturally unstable. It was eroded by acid, leading to the oxidation of iron and the formation of a variety of oxidation products. On the contrary, it could be observed that in the presence of the FATG compound, there only appeared a small number of crystals of corrosion product $FeCl_3$ on the surface, and the peak value corresponding to the iron still maintained a high level. This was consistent with the results of the SEM-EDX. It could be seen that the FATG corrosion inhibitors could prompt the anchor to form a dense protective coating on the metal surface to reduce the contact between the corrosion medium and the metal surface.[40,54]

3.7 Biodegradability

The surfactant used in the metal corrosion inhibitor would inevitably be transferred quantitatively into the environment.

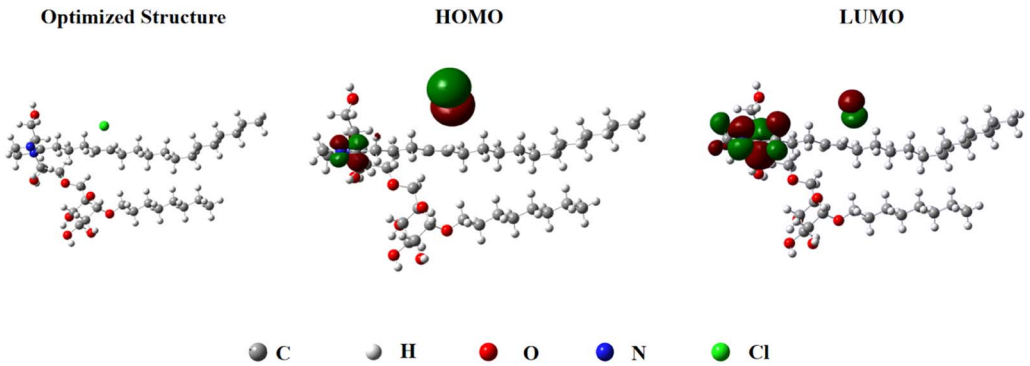

Fig. 11 Optimized geometry of FATG in the solvent, HOMO orbitals, and LUMO orbitals.

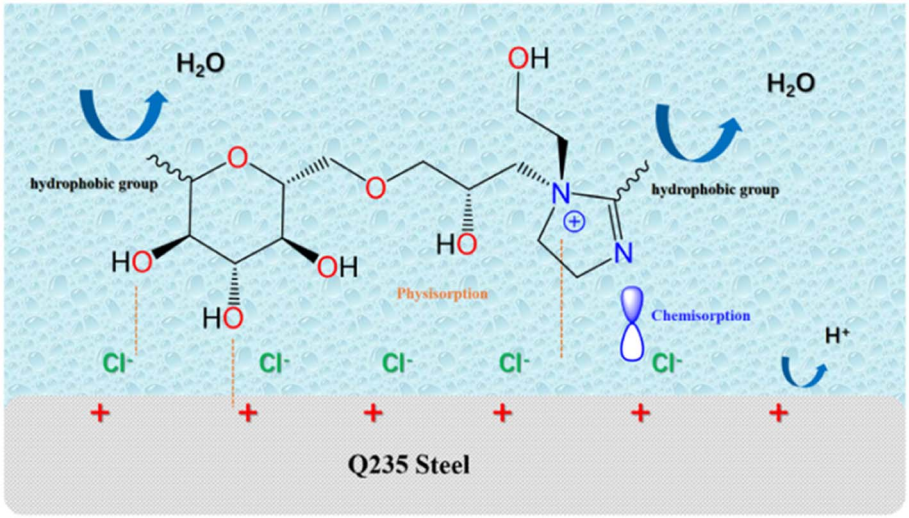

Fig. 12 Corrosion inhibition mechanism of FATG.

Therefore, it was of great significance to study the biodegradation of the FATG surfactant. Under natural conditions or artificial control, the life process of organisms could be decomposed or converted into small molecules. In this study, the biodegradability of the inhibitor was evaluated by the Golden orange-2 method in 28 days. The results showed that its biodegradability was 98.4%, which was higher than previously reported.[55] FATG showed excellent biodegradable properties, probably due to the rapid biodegradation of imidazolinium compounds and alkyl glycosides.[56]

3.8 Quantum chemical calculations

The use of density functional theory (DFT) to evaluate the corrosion inhibition mechanism is an important method.[57] According to quantum chemical calculations, the optimal structure and molecular frontier orbital (HOMO, LUMO) distribution of FATG are presented in Fig. 11. The image of the HOMO showed that the electron cloud surrounded the double bond, which could provide electrons to some of the acceptor molecules with low energy or vacant electron orbitals. The LUMO image mainly surrounded the field of nitrogen atoms that could accept electrons from the surface of Q235 steel. The calculation results showed that green corrosion inhibition could be achieved by introducing imidazoline into alkyl glycosides since the imidazoline ring and double bonds are the active sites of the inhibitor that could be firmly adsorbed on the Fe surface by giving and receiving electrons.[33]

3.9 Corrosion inhibition mechanism

The working mechanism of the inhibitor is based on the direct or indirect adsorption of the inhibitor molecules on the metal surface, thus reducing the contact of the metal surface with the aggressive medium. Q235 steel in acid solution was naturally unstable so it tended to undergo chemical/electrochemical reactions with erosive media in the environment to form more stable substances such as $FeCl_3$ or Fe_2O_3.[24,42] In this paper, grafting imidazoline molecules on the skeleton of glucose derivatives made the prepared inhibitors rich in oxygen and nitrogen atoms, which allowed a large number of connection sites, thus improving their stability on the metal surface.[22]

Based on quantum chemical calculations and related test experiments, the inhibitive mechanism of FATG on Q235 steel in aerated 1 M HCl solution could be explained as seen in Fig. 12. The C=N double bond in the FATG molecular structure having loan pairs of electrons could be adsorbed by donating electrons to the d-orbitals of Q235 steel in a parallel position. Moreover, heterocyclic atoms such as N atoms were prone to accepting the 4s orbital electrons of Fe atoms to adsorb in an acceptor manner.[58,59] In addition, in acidic media, due to electrostatic interaction, FATG molecules carried ammonium cations, which could be quickly adsorbed in the cathode region of the metal. Subsequently, it was difficult for the H^+ in the acid solution to approach the metal, greatly decreasing the corrosion efficiency.[59,60] Simultaneously, the hydrophobic groups kept water molecules away from metals. Based on the result of the gravimetric measurements, heating would promote the formation of chemical bonding between the N atoms of the inhibitor molecule and the ions on the metal surface; accordingly, the inhibitor was firmly attached to the metal surface. Hence, from what has been discussed above, we may conclude that the FATG molecules were adsorbed on the metal surface by physisorption and chemisorption.

4 Conclusion

In summary, a novel alkyl glycoside cationic imaginary ammonium salt (FATG) was synthesized and used as an environmentally friendly corrosion inhibitor for Q235 in 1 M HCl. The inhibition property of FATG was characterized by using chemical and electrochemical measurements. The results revealed that the inhibition efficiency in the presence of FATG increased with increasing the concentration of the inhibitor. The best

inhibition efficiency was about 96.81% at the concentration of 500 ppm (298 K). The adsorption of FATG on the Q235 steel surface conformed to the Langmuir adsorption isotherm. According to thermodynamic parameters, the value of ΔG_{ads} indicated that it was adsorbed on the metal surface by physisorption and chemisorption. As we expected, the inhibitor could be stably present in the system, building a defensive shield on the metal surface to prevent metal oxidation. Moreover, the results of SEM-EDX and XRD supported the formation of inhibitor film on the metal surface. Quantum chemistry calculations had shown that imidazoline rings and double bonds were active sites of this inhibitor, and they could be firmly adsorbed to the metal surface by supplying electrons to iron atoms and accepting electrons.

Conflicts of interest

There are no conflicts to declare.

Acknowledgements

This work was supported by the National Key R&D Program of China (2022YFD2200802) and the Jiangsu Province Key R&D Program (BE2019111). Authors are grateful to Priority Academic Program Development of Jiangsu Higher Education Institutions (PAPD) for their financial support. Authors are also grateful to Mr Jihuai Tan (Chemical Engineering of Nanjing Forestry University) for his assistance with the manuscript.

References

1 B. S. Hou, Q. H. Zhang, Y. Y. Li, G. Y. Zhu, Y. Lei, X. Wang, H. F. Liu and G. A. Zhang, *Corros. Sci.*, 2021, **181**, 109236.
2 Z. Yakun, L. F. Michael, W. Richard and D. William, *Prog. Mater. Sci.*, 2017, **90**, 159–223.
3 G. Cui, Z.-X. Bi, S.-H. Wang, J.-G. Liu, X. Xing, Z.-L. Li and B.-Y. Wang, *Prog. Org. Coat.*, 2020, **148**, 105821.
4 Y.-S. Kim, J. Kim, D. Choi, J.-Y. Limd and J.-G. Kim, *Eng. Anal. Bound. Elem.*, 2017, **77**, 36–48.
5 H.-G. Liu, C.-Y. Chen, X. Yuan, Y. Tan, G.-Z. Meng, H.-F. Liu and Y. F. Cheng, *Corros. Sci.*, 2022, **203**, 110345.
6 W.-C. Zhuang, X.-Q. Wang, W.-Y. Zhu, Y. Zhang, D. Sun, R. Zhang and C.-Y. Wu, *ACS Omega*, 2021, **6**, 5653–5660.
7 M. M. Shaban, N. A. Negm, R. K. Farag, A. A. Fadda, A. E. Gomaa, A. A. Farag and M. A. Migahed, *J. Mol. Liq.*, 2022, **351**, 118610.
8 L. Guo, S. Kaya, I. B. Obot, X.-W. Zheng and Y.-J. Qiang, *J. Colloid Interface Sci.*, 2017, **506**, 478–485.
9 N. A. Negm, F. M. Ghuiba and S. M. Tawfik, *Corros. Sci.*, 2011, **53**, 3566–3575.
10 J. Sinko, *Prog. Org. Coat.*, 2001, **42**, 267–282.
11 L. Ning, D.-D. Wang, L.-X. Wang, L.-F. Wu, J.-Y. Yang, X.-M. Wang, H.-Y. Ma, S.-Y. Feng and H.-F. Lu, *Silicon*, 2020, **12**, 1455–1468.
12 N. B. Guzman, D. M. Escalera, J. P. Calderon, J. G. Rodriguez and L. M. Gomez, *Green Chem. Lett. Rev.*, 2019, **12**, 49–61.
13 G. S. Solano, J. P. Calderonc, L. M. Escalera, J. Canto, M. C. Diaz, O. S. Mazon, J. Henao and L. M. Gomez, *Ind. Crops Prod.*, 2018, **119**, 111–124.
14 E. R. Dorantes, J. Z. Díaz, A. Q. Hernandez, J. P. Calderon, J. G. Rodriguez and L. M. Gomez, *J. Chem.*, 2017, 2871034.
15 E. S. Salazar, E. V. Velez, J. Uruchurtu, J. P. Calderon, M. Casales, I. R. Cadena, R. L. Cecenes and J. G. Rodriguez, *Mater*, 2021, **14**, 4206.
16 A. C. Zabalegui, E. V. Velez, G. G. Aguilar, M. C. Diaz, R. L. Sesenes, J. G. Rodriguez and L. M. Gomez, *Ind. Crops Prod.*, 2019, **133**, 203–211.
17 Z. Sanaeia, M. Ramezanzadeha, G. Bahlakehb and B. Ramezanzadeh, *J. Ind. Eng. Chem.*, 2018, 4159.
18 P. B. Raja and M. G. Sethuraman, *Mater. Lett.*, 2008, **62**, 113–116.
19 V. Srivastava, D. S. Chauhan, P. G. Joshi, V. Maruthapandian, A. A. Sorour and M. A. Quraishi, *ChemistrySelect*, 2018, **3**, 1990–1998.
20 M. Mobin, M. Khan and M. Parveen, *J. Appl. Polym. Sci.*, 2011, **121**, 1558–1565.
21 C. Verma and M. Quraishi, *Int. J. Biol. Macromol.*, 2021, **184**, 118–134.
22 X. Wang, Y. Lei, Z.-N. Jiang, Q.-H. Zhang, Y.-Y. Li, H.-F. Liu and G.-A. Zhang, *Ind. Crops Prod.*, 2022, **188**, 115680.
23 M. Rbaa, F. Benhib, R. Hssisou, Y. Lakhrissi, B. Lakhrissi, M. E. Touhami, I. Warad and A. Zarrouk, *J. Mol. Liq.*, 2021, **322**, 114549.
24 D. S. Chauhan, A. M. Kumar and M. A. Quraishi, *Chem. Eng. Res. Des.*, 2019, **150**, 99–115.
25 S. Banerjee, V. Srivastava and M. M. Singh, *Corros. Sci.*, 2012, **59**, 35–41.
26 M. M. Solomon, S. A. Umoren, I. B. Obot, A. A. Sorour and H. Gerengi, *ACS Appl. Mater. Interfaces*, 2018, **10**, 28112–28129.
27 M. Mobin and M. Rizvi, *Carbohydr. Polym.*, 2017, **160**, 172–183.
28 X.-F. Liu and X.-Y. Cao, *Adv. Mater. Res.*, 2013, **781**, 72–75.
29 J.-H. Tan, Q.-H. Fu, Y.-Q. Qu, F. Wang, W.-G. Wang, F. Wang, Y.-F. Cao and X.-B. Zhu, *J. Cleaner Prod.*, 2021, **289**, 125821.
30 X. Lu, *Adv. Mater. Res.*, 2016, **521**, 629–632.
31 Y. Huang, X.-W. Zhou, L.-S. Fang, Z.-R. Jia, Z.-Z. Yu and X.-B. Zhu, *Fine Chem.*, 2021, **38**, 2312–2321.
32 B. Lin, J.-X. Wang, H.-L. Zhang, Y.-Y. Wang, H.-L. Zhang, J.-L. Tang, J. Hou, H.-B. Zhang and M.-X. Sun, *Corros. Sci.*, 2022, **197**, 110084.
33 M. Behpour, S. M. Ghoreishi, N. Soltani, M. S. Niasari, M. Hamadanian and A. Gandomi, *Corros. Sci.*, 2008, **50**, 2172–2181.
34 F. G. Liu, M. Du, J. Zhang and M. Qiu, *Corros. Sci.*, 2009, **51**, 102–109.
35 A. Fitoz, H. Nazır, M. Özgür, E. Emregül and K. C. Emregül, *Corros. Sci.*, 2018, **133**, 451–464.
36 W.-T. Xu, J.-X. Wei, Z.-G. Yang, P. Xu and Q.-J. Yu, *Constr. Build. Mater.*, 2020, **250**, 118861.
37 L.-R. Ma, W.-Q. Lu, D. Yang, J.-J. Shen, Z.-S. Gao, S.-Y. Zhang and Q.-Q. Liao, *Sustainable Chem. Pharm.*, 2021, **22**, 100488.

38 C. Bonaccorso, G. Grasso, N. Musso, V. Barresi, D. F. Condorelli, D. La Mendol and E. Rizzarelli, *J. Inorg. Biochem.*, 2018, **182**, 92–102.
39 M. P. Sathisha, S. Budagumpi, N. V. Kulkarni, G. S. Kurdekar, V. K. Revankar and K. S. R. Pai, *Eur. J. Med. Chem.*, 2010, **45**, 106–113.
40 M. A. Migahed, E. G. Zaki and M. M. Shaban, *RSC Adv.*, 2016, **6**, 71384–71396.
41 M. Mobin and M. Rizvi, *Carbohydr. Polym.*, 2017, **160**, 172–183.
42 H.-Y. Wei, B. Heidarshenas, L.-S. Zhou, G. Hussain, Q. Li and K. Ostrikov, *Mater. Today Sustain.*, 2020, **10**, 100044.
43 S. Satpati, A. Suhasaria, S. Ghosal, A. Saha, S. Dey and D. Sukul, *J. Mol. Liq.*, 2021, **324**, 115077.
44 A. Fitoz, H. Nazır, M. Özgür, E. Emregül and K. C. Emregül, *Corros. Sci.*, 2018, **133**, 451–464.
45 G. Bahlakeh, B. Ramezanzadeh, A. Dehghani and M. Ramezanzadeh, *J. Mol. Liq.*, 2019, **283**, 174–195.
46 F. Bentiss, M. Traisnel and M. Lagrenee, *Corros. Sci.*, 2000, **42**, 127–146.
47 D. K. Yadav, D. S. Chauhan, I. Ahamad and M. A. Quraishi, *RSC Adv.*, 2013, **3**, 632–646.
48 M. Bouanis, M. Tourabi, A. Nyassi, A. Zarrouk, C. Jama and F. Bentiss, *Appl. Surf. Sci.*, 2016, **389**, 952–966.
49 G. Bahlakeh, B. Ramezanzadeh, A. Dehghani and M. Ramezanzadeh, *J. Mol. Liq.*, 2019, **283**, 174–195.
50 A. Yurt, S. Ulutas and H. Dal, *Appl. Surf. Sci.*, 2006, **253**, 919–925.
51 A. Döner and G. Kardas, *Corros. Sci.*, 2011, **53**, 4223–4232.
52 M. Ouakki, M. Galai, M. Rbaa, A. S. Abousalem, B. Lakhrissi, M. E. Touhami and M. Cherkaoui, *J. Mol. Liq.*, 2020, **319**, 114063.
53 A. S. Fouda, M. A. Ismail, A. M. Temraza and A. S. Abousalem, *New J. Chem.*, 2019, **43**, 768–789.
54 Y. Hua, S.-S. Xu, Y. Wang, W. Taleb, J.-B. Sun, L. Zhang, R. Barkera and A. Neville, *Corros. Sci.*, 2019, **157**, 392–405.
55 I. T. Gawali and G. A. Usmani, *J. Dispersion Sci. Technol.*, 2020, **41**, 450–460.
56 D. Bajpal and V. K. Tyagi, *J. Oleo Sci.*, 2006, **55**, 319–329.
57 A. Zarrouk, H. Zarrok, Y. Ramli, M. Bouachrine, B. Hammouti, A. Sahibed and F. Bentiss, *J. Mol. Liq.*, 2016, **222**, 239–252.
58 L.-R. Ma, W.-Q. Lu, D. Yang, J.-J. Shen, Z.-S. Gao, S.-Y. Zhang and Q.-Q. Liao, *Sustainable Chem. Pharm.*, 2021, **22**, 100488.
59 C. Vermal, E. E. Ebenso, M. A. Quraishil and C. M. Hussain, *Mater. Adv.*, 2021, **2**, 3806–3850.
60 R. O. Medupin, K. Ukoba, K. O. Yoro and T. C. Jen, *Mater. Today Sustain.*, 2023, **5**, 100373.